Electronic Supplementary Material (ESI) for Polymer Chemistry.

SUPPLEMENTARY INFORMATION

Dispersity and Architecture Driven Bulk Phase Behavior and Confined Crystallization In Symmetric Branched Block Copolymers Containing Polylactide and Polycyclooctene

Louis M. Pitet[†§*], Bradley M. Chamberlain[‡], Adam W. Hauser[†] and Marc A. Hillmyer[†*]

[†]*Department of Chemistry, University of Minnesota, 207 Pleasant St. SE, Minneapolis, Minnesota 55455-0431, United States,* [§]*Institute for Materials Research (IMO) and Department of Chemistry, Hasselt University, Martelarenlaan 42, 3500 Hasselt, Belgium* [‡]*Department of Chemistry, Luther College, 700 College Drive, Decorah, Iowa 52101, United States*

EXPERIMENTAL DETAILS

Materials

Tetrahydrofuran and toluene (Mallinkrodt) were passed through an activated alumina column under nitrogen to remove protic impurities. All other reagent grade solvents were used without further purification. *cis*-cyclooctene (COE), (IMesH_2)-(Cy_3P)$RuCl_2$(CHPh) (Grubbs second generation catalyst, G2), tin(II) ethylhexanoate ($Sn(Oct)_2$), 2,2′-bis(hydroxymethyl)propionic acid (bisMPA), dicyclohexylcarbodiimide (DCC), para-toluenesulfonic acid monohydrate (pTSA), DOWEX® 50W-100X cation exhchange resin, and 4-(dimethylamino)pyridine (DMAP) were all purchased from Aldrich. 2,2-dimethoxypropane was purchased from Fluka. COE was distilled over CaH_2 prior to use. All other chemicals were used as received. Synthesis of all polymers has been described in detail in a previous article.[1]

Characterization

NMR

^{1}H-NMR spectroscopy was performed on a Varian Inova 500 instrument operating at 500 MHz. Solutions were prepared in either DMSO-d_6 for chain-transfer agents or $CDCl_3$ (Cambridge Isotope Laboratories) for polymers at approximately 15 mg/mL. All spectra were obtained at 20 °C after 64 transients using a relaxation delay of 5 s with chemical shifts reported as (ppm) relative to the ^{1}H signals from hydrogenous solvent (7.27 ppm for $CHCl_3$; 2.50 ppm for DMSO).

SEC

Size-exclusion chromatography (SEC) was used to evaluate the molecular weight evolution and polydispersity index in the triblock copolymers. Two different instruments were used based on the availability of different detectors. In one case, samples were prepared at concentrations near 1 mg/mL in $CHCl_3$. The instrument operates at 35 °C using three Plgel 5μm Mixed-C columns in series with molecular weight range 400–400 000 g mol^{-1}. The columns are housed in a Hewlett-Packard (Agilent Technologies) 1100 series liquid chromatograph equipped with a Hewlett-Packard 1047A refractive index detector. Molar mass dispersities, *Đ,* are reported with respect to polystyrene standards obtained from Polymer Laboratories. Alternatively, polymer solutions were prepared in tetrahydrofuran and injected onto an instrument housing three Phenomenex Phenogel columns operating at 30 °C. The characteristics were evaluated from responses from two detectors; one Wyatt Technology Dawn DSP Multi-angle Laser Photometer with a 633 nm He-Ne laser and one Optilab rEX Interfermometric refractometer. The flow rate of this instrument is 1 mL/min, maintained by an Alltech 426 HPLC positive displacement pump. The data evaluation for molecular weight calculations is performed using ASTRA software from Wyatt Technology.

DSC

Differential scanning calorimetric (DSC) analysis was performed on a Q1000 instrument from TA Instruments calibrated with an Indium standard. Samples were initially heated to

160 °C and held isothermally for 5 min to remove discrepancies originating from variable thermal history. The samples were subsequently cooled to –120 °C at a rate of 10 °C min^{-1} followed by heating to 120 °C again at a rate of 10 °C min^{-1}; data from the second heating cycle is presented in the supporting information, in order to establish the melting temperature independent from thermal history. Crystallization data is presented in the main body of the manuscript during the cooling cycle at 10 °C min^{-1}. Data analysis (T_m; T_c; $T_{g,L}$; $\Delta H_{m,C}$; $\Delta H_{c,C}$ was performed using Universal Analysis software from TA Instruments.

TEM

Ultrathin sections (ca. 70 nm) of the polymer samples were microtomed using a Reichert UltraCut S Ultramicrotome with a Model FC-S addition, enabling microtoming at –120 °C, well below the lowest T_g. The thin sections were mounted on 400 mesh copper grids and stained with OsO4 vapor for 15 min from a 4% aqueous solution. Transmission electron microscopy (TEM) was performed on a JEOL JEM-1210 microscope operating at 120 keV. Images were captured with a Gatan Multiscan CCD camera.

SAXS

Small-angle X-ray scattering experiments were performed at the Advanced Photon Source (APS) at Argonne National Laboratories at Sector 5-ID-D beamline. The beamline

is maintained by the Dow-Northwestern-Dupont Collaborative Access Team (DND- CAT). The source produces X-rays with a wavelength of 0.73 Å. The sample to detector distance was 6.52 m and the detector diameter was 165 mm. Scattering intensity was monitored by a Mar 165 mm diameter CCD detector with a resolution of 2048 × 2048. The two-dimensional scattering patterns were azimuthally integrated to afford one-dimensional profiles presented as scattered intensity (I) versus scattering wavevector (q).

Table S1. Sample IDs and thermal properties for a series of linear, H-shaped, and arachnearm block polymers

Sample ID	w_L	f_L	f_C	$T_{g,L}$ (°C)	$T_{g,C}$ (°C)	T_m (°C)	ΔH_m (J/g)	T_c (°C)	ΔH_c (J/g)	X_C (%)
LINEAR										
HO–C–OH	0.00	0.00	1.00	–	–66	58	64	38	66	31
LCL [1.5–22–1.5]	0.12	0.09	0.91	–	–69	58	54	34	62	33
LCL [4–22–4]	0.27	0.20	0.80	31	–71	49	36	27	40	25
LCL [6–22–6]	0.37	0.29	0.71	38	–70.9	49	28	28	32	24
LCL [10–22–10]	0.46	0.38	0.62	42	–71	50	18	29	29	25
LCL [17–22–17]	0.60	0.51	0.49	41	–72	47	16	25.7/–9	19	22
LCL [21–22–21]	0.66	0.57	0.43	42	–76	46	12	28.6/–3	13	17
LCL [37–22–37]	0.77	0.70	0.30	42	–73	47	14	3.3/–10	13	25
LCL [62–22–62]	0.85	0.80	0.20	42	–86	50	3.0	–10.7	5.1	16
H-SHAPED										
HO_2–C–OH_2	0.00	0.000	1.00	–	–66.2	56	62	37	68	31
L_2CL_2 [0.7_2–23–0.7_2]	0.13	0.096	0.90	–	–	–	–	–	–	–
L_2CL_2 [2_2–23–2_2]	0.26	0.192	0.81	34	–69.6	49	44	25.9	43	26
L_2CL_2 [3_2–23–3_2]	0.36	0.285	0.72	37	–71.8	48	26	26.8/–5	34	25
L_2CL_2 [5_2–23–5_2]	0.46	0.373	0.63	38	–73.5	47	23	21/–7	28	24
L_2CL_2 [8_2–23–8_2]	0.58	0.494	0.51	42	–72.4	44	16	27.5/–2	18	20
L_2CL_2 [10_2–23–10_2]	0.66	0.574	0.43	43	–74.2	47	15	–6.4	18	24
L_2CL_2 [17_2–23–17_2]	0.76	0.688	0.31	42	–73.9	44	9	1.8/–11	9	17
L_2CL_2 [30_2–23–30_2]	0.85	0.794	0.21	44	–	48	8.0	–8.4	8.1	25
ARACHNEARM										
HO_4–C–OH_4	0.00	0.00	1.00	–	–72.1	58	67	34.6	68	31
L_4CL_4 [0.4_4–27–0.4_4]	0.12	0.08	0.92	–	-69.6	56	44	32.76	52	27
L_4CL_4 [1_4–27–1_4]	0.19	0.14	0.86	33	–75.7	58	43	32	47	27
L_4CL_4 [2_4–27–2_4]	0.36	0.28	0.72	37	-70.91	52	27	30.4	35	25
L_4CL_4 [3_4–27–3_4]	0.44	0.36	0.64	40	–77.6	52	23	–8/29.5	28	23
L_4CL_4 [5_4–27–5_4]	0.58	0.49	0.51	42	-74.46	51	18	–5.15	23	26
L_4CL_4 [6_4–27–6_4]	0.65	0.56	0.44	43	–78.2	52	3.0	–5.7	15	19
L_4CL_4 [11_4–27–11_4]	0.77	0.70	0.30	44	-75.2	50	7.4	–6.14	7	15
L_4CL_4 [19_4–27–19_4]	0.85	0.80	0.20	44	–76.3	55	4.5	–6.3	6.5	20

PHASE DIAGRAMS

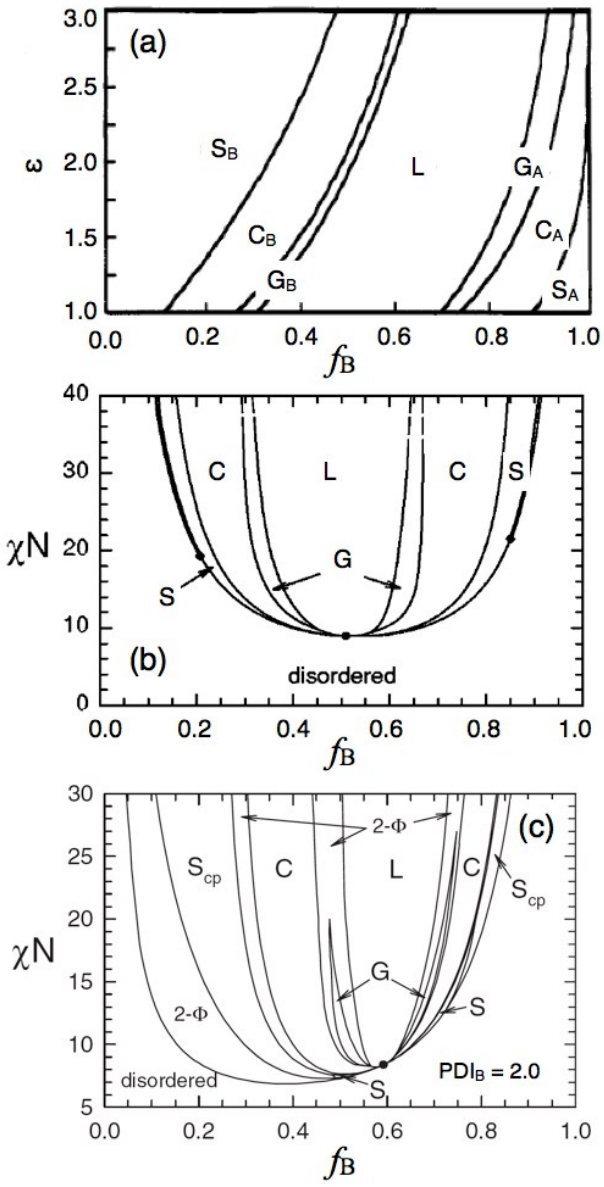

Figure S1. Theoretical phase diagrams constructed from mean-field theory for (a) monodisperse A_xB block copolymers, (b) conformationally symmetric, monodisperse, symmetric ABA triblock copolymers, and (c) conformationally symmetric AB diblock copolymers with PDI_A = 1.0 and PDI_B = 2.0 (Notably, relatively large windows of biphasic morphologies are predicted (2-Φ), as a result of macrophase separation). The x-axis in each plot corresponds to the volume fraction of the B-component (f_B). Reproduced from references (a) [2], (b) [3], and (c) [4]

Conformational asymmetry alone has been shown to govern the position of the phase boundaries with respect to volume fraction to a moderate extent.[5-9]

$$\epsilon = \left(\frac{n_B}{n_A}\right)\left(\frac{\beta_A}{\beta_B}\right) \quad (1)$$

A more flexible chain inherently has smaller root mean squared radius of gyration, which would consequently give a smaller value of β. There is a greater entropic penalty to stretch a more flexible chain and this in turn causes curvature away from the more flexible component to avoid excessive stretching of that block. Therefore, both increased flexibility and increased functionality of one component (A) at a junction both cause a shift in the phase boundary of the theoretical phase diagram toward higher volume fraction of the other component (B).[2, 6, 7, 10, 11]

In the strongly segregated system described in this work, there is a strong tendency to minimize the interfacial area per chain; individual chains stretch relatively far from the covalent junction and thereby sharpen the A/B interface.[12]. A compositionally symmetric system can compensate for this excessive stretching penalty by spontaneously adjusting the interfacial curvature inward toward the A domain, thereby accommodating the larger volume necessary for the two B-type chains to relax.[13]

Compared with the influence of branching, the phase boundaries are shifted modestly with respect to composition by the symmetric triblock architecture compared with a simple monodisperse AB diblock copolymer.

STATISTICAL PARAMETERS (OR CONFORMATIONAL SYMMETRY)

Statistical Parameters for PCOE–PLA Block Copolymers

The statistical parameters for the system investigated in this report were taken from previous determinations. The standard reference volume (v_i), with which segment lengths are calculated throughout the remaining text, was taken based on a four-carbon repeating unit, with the temperature dependence considered according to eq 2.

$$v_i = 1.084 \times 10^{-22} \cdot e^{6.85\times10^{-4}(T-296)]} \quad (2)$$

Importantly, the temperature dependence of the reference volume only effects the value slightly over the experimentally relevant temperature range: v_i (25 °C) = 108 Å^3 and v_i (140 °C) = 112 Å^3. The statistical segment lengths (a_i) for the two components were acquired by different methods. For PLA, the root-mean square (RMS) end-to-end distance ($\langle h^2 \rangle_0$) was determined from neutron scattering. The ratio $\langle h^2 \rangle_0/M$ was calculated to be 0.699 at 30 °C and 0.554 at 200 °C.[14] Statistical segment length for PLA (a_L) is calculated from this measurement according to eq 3.

$$\frac{< h^2 >_0}{M} = \frac{Na^2}{M} = \frac{a^2}{m_o} \quad (3)$$

where N is the number average repeating units of volume v_i, and correspondingly m_o is the molecular weight of the component contained within the reference volume. The value of m_o for PLA is 81.4 g mol^{-1} at 25 °C and is 77.6 g mol^{-1} at 200 °C as calculated using the polymer density determined by Witzke and coworkers.[15] This leads to a value of a_L equal to 7.6 Å at 25 °C and 6.5 Å at 200 °C.

The RMS end-to-end distance has not been directly measured for PCOE. However, the value can be estimated by taking an intermediate value between the measured values for polyethylene (PE) and 1,4-polybutadiene (PBD). The measured values of ($<h^2>_0$) for PE at 25 °C and 140 °C were 1.42 and 1.25 Å mol g^{-1}, respectively. According to equation 3, this provides values of statistical segment length a_E equal to 8.9 and 8.4 Å at temperatures of 25 and 140 °C, respectively, using the repeating unit molecular weight within a volume v_i of 56 g mol^{-1} ($\rho_{25\,°C}$ = 0.85 g mL^{-1}; $\rho_{140\,°C}$ = 0.79 g mL^{-1}).[16, 17] Likewise, the statistical segment lengths for PBD at 25 °C and 140 °C were calculated to be 7.3 Å and 7.2 Å, respectively ($\rho_{25\,°C}$ = 0.89 g mL^{-1}; $\rho_{140\,°C}$ = 0.83 g mL^{-1}).[17] Using this information, it was estimated that the statistical segment length for PCOE (a_C) is approximately 7.8–8.0 Å. Considering this information facilitates the assumption that conformational asymmetry of the system containing PLA and PCOE blocks contributes minimally to the asymmetry in the phase diagram compared with the disparity in functionality at the branching junctions, according to the calculated values of β (eq 4) and substituting into eq 1. Considering the conformational asymmetry in a similar system comprised of linear diblock copolymers containing PLA and the hydrocarbon poly(ethylene-*alt*-propylene) lends credence to this assumption. The calculated conformational asymmetry parameter (1.06)[14] and the experimental phase diagram are

consistent with minimal shift in the boundaries separating the ordered morphologies; the phase diagram is nearly perfectly symmetric across f_{PLA} = 0.50 isopleth.[14, 18]

$$\beta_i^2 = \frac{R_g^2}{V_{tot}} = \frac{Na^2}{6V} = \frac{a_i^2}{6v_i} = \frac{a^2 \rho N_A}{6m_o} = \frac{< h^2 >_0}{M} \cdot \rho N_A \qquad (4)$$

MOLAR MASS DISPERSITY

Simple AB diblock copolymers having blocks with different molar mass distributions have been theoretically[4, 5, 19-25] and experimentally[26-33] investigated. Ruzette and coworkers disclosed the morphological ramifications of polydisperse end-blocks in symmetric ABA-type triblock copolymers.[30] The high dispersity ($Đ$ ~ 1.5) in the endblock comprised of poly(methyl methacrylate) (PMMA) caused an apparent shift in phase boundaries toward higher volume fraction of the midblock poly(butyl acrylate) (PBA) compared with monodisperse systems. For example, lamellar morphologies were suggested by TEM micrographs in samples where PMMA comprised the majority (f_{PMMA} = 0.58), and a poorly organized cylindrical phase was observed with f_{PMMA} = 0.50 (PMMA cylinders). The shift in morphological boundaries and spontaneous curvature toward PMMA at nearly symmetric composition was attributed to the disparity in molecular weight distributions, considering the nearly symmetric conformational characteristics (conformational asymmetry = 1.17). Notably, the polymers investigated were all relatively high molecular weight (M_n range 80–100 kg mol^{-1}).

Fairly recently, symmetric linear ABA-type triblock copolymers with a high dispersity midblock were synthesized [1, 34-36] and in some cases evaluated for morphological features

by transmission electron microscopy (TEM) and small-angle x-ray scattering (SAXS).[37-39] The results are generally consistent with expectations based on mean-field theory for triblocks with comparatively large midblock dispersity.[40]

Adjusting the dispersity in the end-block of ABC triblock terpolymers has also been shown to induce transitions between different ordered morphologies.[41, 42] Increasing *Đ* effectively reduces the stretching energy penalty for an ensemble of polymer chains. In essence, this translates to the spontaneous curvature of the A-B interface inward toward the more highly disperse block, corresponding to the PCOE midblock in our B_xAB_x system. The predicted feature of shifting the phase boundary on the theoretical phase diagrams toward higher volume fraction of A (PCOE) moves in the same direction as that caused by asymmetry in junction functionality (x > 1). The combined *Đ*-disparity and branched architectures are predicted to exacerbate the phase-boundary shift and may lead to certain morphologies being adopted at compositions unprecedented in previous experimental reports.

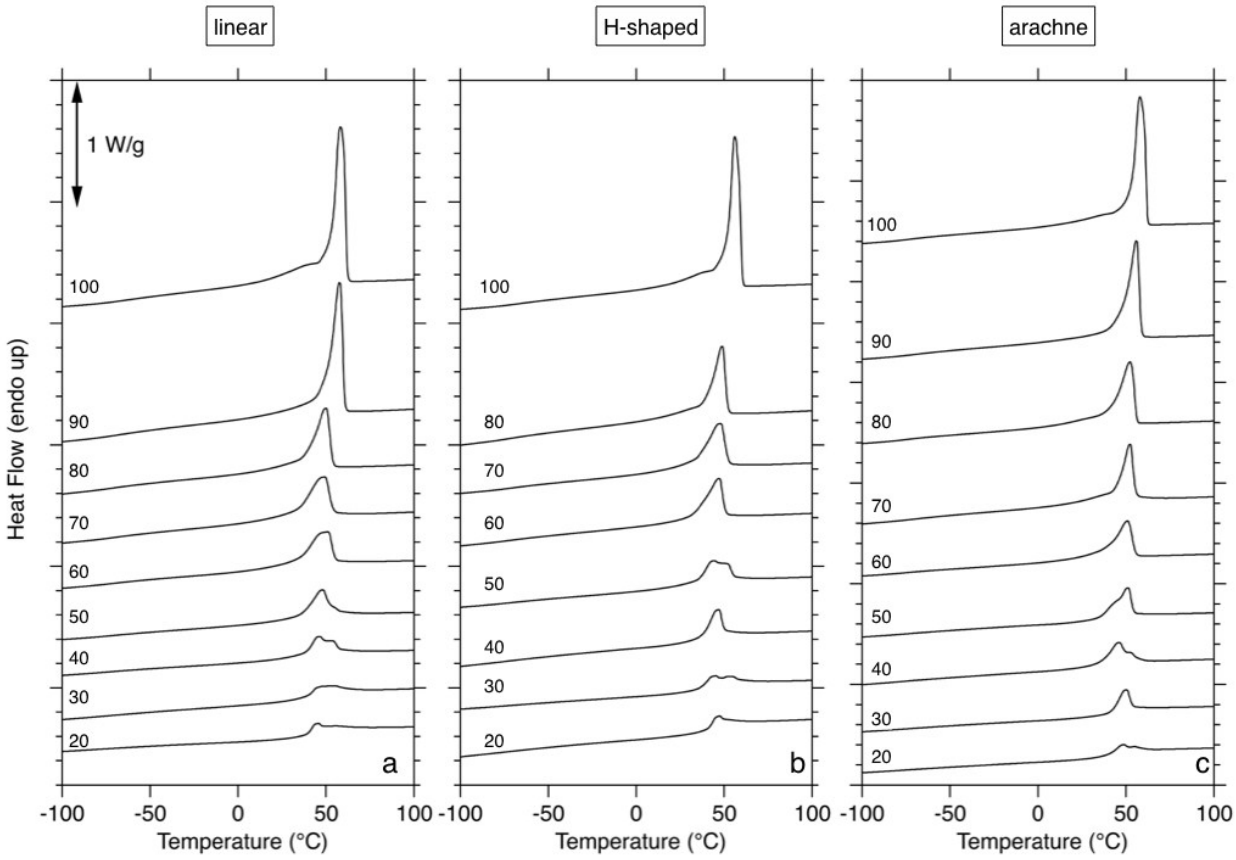

Figure S2. DSC thermograms for heating (10 °C/min) of (a) linear (b) H-shaped and (c) arachnearm block polymers with the numbers indicating the content of PCOE (%) in the sample.

REFERENCES

1. L. M. Pitet, B. M. Chamberlain, A. W. Hauser and M. A. Hillmyer, *Macromolecules*, 2010, **43**, 8018-8025.
2. S. T. Milner, *Macromolecules*, 1994, **27**, 2333-2335.
3. M. W. Matsen and R. B. Thompson, *J. Chem. Phys.*, 1999, **111**, 7139–7146.
4. M. W. Matsen, *Eur. Phys. J. E: Soft Matter*, 2006, **21**, 199-207.
5. E. Helfand and Z. R. Wasserman, *Developments in Block Copolymers*, 1982, **1**, 99-125.

6. C. Lai, W. B. Russel, R. A. Register, G. R. Marchand and D. H. Adamson, *Macromolecules*, 2000, **33**, 3461-3466.
7. M. W. Matsen and F. S. Bates, *J. Polym. Sci., Part B: Polym. Phys.*, 1997, **35**, 945-952.
8. J. D. Vavasour and M. D. Whitmore, *Macromolecules*, 1993, **26**, 7070-7075.
9. F. S. Bates, M. F. Schulz, A. K. Khandpur, S. Foerster and J. H. Rosedale, *Faraday Discuss.*, 1994, **98**, 7-18.
10. K. Almdal, M. A. Hillmyer and F. S. Bates, *Macromolecules*, 2002, **35**, 7685-7691.
11. M. W. Matsen and M. Schick, *Macromolecules*, 1994, **27**, 4014-4015.
12. E. Helfand and Z. R. Wasserman, *Macromolecules*, 1976, **9**, 879-888.
13. M. W. Matsen and F. S. Bates, *Macromolecules*, 1996, **29**, 7641-7644.
14. K. S. Anderson and M. A. Hillmyer, *Macromolecules*, 2004, **37**, 1857-1862.
15. D. R. Witzke, J. J. Kolstad and R. Narayan, *Macromolecules*, 1997, **30**, 7075-7085.
16. L. J. Fetters, D. J. Lohse and W. W. Graessley, *J. Polym. Sci., Part B: Polym. Phys.*, 1999, **37**, 1023-1033.
17. L. J. Fetters, D. J. Lohse, D. Richter, T. A. Witten and A. Zirkel, *Macromolecules*, 1994, **27**, 4639-4647.
18. S. C. Schmidt and M. A. Hillmyer, *J. Polym. Sci., Part B: Polym. Phys.*, 2002, **40**, 2364-2376.
19. T. M. Beardsley and M. W. Matsen, *European Physical Journal E*, 2008, **27**, 323-333.
20. S. T. Milner, T. A. Witten and M. E. Cates, *Macromolecules*, 1988, **21**, 2610-2619.
21. S. T. Milner, T. A. Witten and M. E. Cates, *Macromolecules*, 1989, **22**, 853-861.
22. S. T. Milner, *J. Polym. Sci., Part B: Polym. Phys.*, 1994, **32**, 2743-2755.
23. A.-C. Shi and J. Noolandi, *Macromolecules*, 1994, **27**, 2936-2944.
24. G. H. Fredrickson and E. Helfand, *J. Chem. Phys.*, 1987, **87**, 697-705.
25. S. W. Sides and G. H. Fredrickson, *J. Chem. Phys.*, 2004, **121**, 4974-4986.
26. J. M. Widin, M. Kim, A. K. Schmitt, E. Han, P. Gopalan and M. K. Mahanthappa, *Macromolecules*, 2013, **46**, 4472-4480.
27. N. A. Lynd and M. A. Hillmyer, *Macromolecules*, 2005, **38**, 8803-8810.
28. N. A. Lynd and M. A. Hillmyer, *Macromolecules*, 2007, **40**, 8050–8055.

29. D. Bendejacq, V. Ponsinet, M. Joanicot, Y. L. Loo and R. A. Register, *Macromolecules*, 2002, **35**, 6645-6649.
30. A.-V. Ruzette, S. Tence-Girault, L. Leibler, F. Chauvin, D. Bertin, O. Guerret and P. Gerard, *Macromolecules*, 2006, **39**, 5804-5814.
31. M. Nadgorny, D. T. Gentekos, Z. Y. Xiao, S. P. Singleton, B. P. Fors and L. A. Connal, *Macromol. Rapid Commun.*, 2017, **38**, 1700352.
32. D. T. Gentekos and B. P. Fors, *Acs Macro Letters*, 2018, **7**, 677-682.
33. D. T. Gentekos, J. T. Jia, E. S. Tirado, K. P. Barteau, D. M. Smilgies, R. A. DiStasio and B. P. Fors, *J. Am. Chem. Soc.*, 2018, **140**, 4639-4648.
34. S. M. Banik, B. L. Monnot, R. L. Weber and M. K. Mahanthappa, *Macromolecules*, 2011, **44**, 7141-7148.
35. M. K. Mahanthappa, F. S. Bates and M. A. Hillmyer, *Macromolecules*, 2005, **38**, 7890-7894.
36. L. M. Pitet and M. A. Hillmyer, *Macromolecules*, 2009, **42**, 3674–3680.
37. J. M. Widin, A. K. Schmitt, K. Im, A. L. Schmitt and M. K. Mahanthappa, *Macromolecules*, 2010, **43**, 7913-7915.
38. J. M. Widin, A. K. Schmitt, A. L. Schmitt, K. Im and M. K. Mahanthappa, *J. Am. Chem. Soc.*, 2012, **134**, 3834-3844.
39. A. K. Schmitt and M. K. Mahanthappa, *Macromolecules*, 2014, **47**, 4346-4356.
40. M. W. Matsen, *European Physical Journal E*, 2013, **36**, 1-7.
41. A. J. Meuler, C. J. Ellison, J. Qin, C. M. Evans, M. A. Hillmyer and F. S. Bates, *J. Chem. Phys.*, 2009, **130**, 234903/234901-234903/234917.
42. A. J. Meuler, C. J. Ellison, M. A. Hillmyer and F. S. Bates, *Macromolecules*, 2008, **41**, 6272-6275.